JOURNAL OF SOLID STATE CHEMISTRY 95, 29–38 (1991)

Structure and Chemistry of $Ba_{0.6}K_{0.4}BiO_y$ at High Temperature

SHIYOU PEI,* J. D. JORGENSEN,† D. G. HINKS,† YING ZHENG,† D. R. RICHARDS,* B. DABROWSKI,* AND A. W. MITCHELL†

Science and Technology Center for Superconductivity and †Materials Science Division, Argonne National Laboratory, Argonne, Illinois 60439

Received April 15, 1991; in revised form June 7, 1991

A combination of neutron powder diffraction and thermogravimetric analysis has been used to study the structural phase behavior of $Ba_{1-x}K_xBiO_y$ under conditions that simulate synthesis. On heating in 1% O_2, the cubic perovskite $Ba_{0.6}K_{0.4}BiO_3$ decomposes to a mixture of $Ba_{1-x}K_xBiO_y$ with $x < 0.4$ and $KBiO_2$. Further increase in temperature causes the reincorporation of potassium into the perovskite at the expense of $KBiO_2$. At 720°C, the sample is again a single-phase cubic perovskite with $x = 0.4$ containing a large concentration of oxygen vacancies. If this sample is then cooled in argon, no chemical phase decomposition occurs. Instead, the cubic oxygen-deficient perovskite transforms to an orthorhombic oxygen-vacancy-ordered phase. A subsequent low-temperature anneal in pure oxygen fills the oxygen vacancies while retaining the potassium in the lattice, resulting in a transformation back to the cubic perovskite. This work shows that fully oxygenated $Ba_{1-x}K_xBiO_3$ for $x > 0.1$, including the superconducting compositions, is metastable, and supports the hypothesis that the creation of oxygen vacancies is necessary to allow the substitution of K^{1+} for Ba^{2+} in the lattice.

I. Introduction

The perovskite compound $Ba_{1-x}K_xBiO_3$, with $T_c = 30$ K for $x = 0.4$, is one of the simplest oxide superconductors known to date (*1–3*). However, the synthesis of this material is not straightforward. Early attempts to synthesize this material in oxygen failed (*1–3*). Hinks *et al.* (*3*) later showed that the single-phase material could only be synthesized by firing the material in a reducing atmosphere, followed by a low-temperature anneal in oxygen to fill oxygen vacancies created during the initial firing. Based on charge-neutrality considerations, they assumed that the creation of oxygen vacancies in $Ba_{1-x}K_xBiO_y$ is needed to allow the substitution of K^{1+} for Ba^{2+}.

The aim of the present work is to investigate both the structural and chemical phase behavior of $Ba_{1-x}K_xBiO_y$ at high temperature in order to understand the synthetic chemistry of this material. A combination of neutron powder diffraction (NPD) and thermogravimetric analysis (TGA) is used in this study. An investigation of the complete phase diagram of $Ba_{1-x}K_xBiO_y$ vs x, temperature and oxygen partial pressure is beyond the scope of this work. Rather, we have concentrated on the superconducting composition near $x = 0.4$.

II. Experimental

$Ba_{0.6}K_{0.4}BiO_3$ was prepared by the melt-process technique described previously (*4*).

0022-4596/91 $3.00

In order to prepare a sample with geometry suitable for *in situ* neutron powder diffraction, the material was ground into a powder and pressed into pellets 10 mm in diameter and approximately 7 mm in height. The pellets were then fired in nitrogen gas at 700°C. A subsequent anneal at 400°C in flowing O_2 with slow cooling to room temperature was performed to fully oxygenate the material.

For the *in situ* neutron powder diffraction experiment, pellets were stacked to form a 50-mm-high, free-standing sample that was placed into a controlled-atmosphere furnace designed for time-of-flight neutron powder diffraction experiments (*5*). The oxygen content of the furnace environment was controlled by a flowing (200–400 cm^3/min) mixture of oxygen–argon at atmospheric pressure. Neutron powder diffraction data were collected on the special environment powder diffractometer (SEPD) at Argonne's intense pulsed neutron source at the $2\theta = 90°$ scattering angle (*6*). At this fixed scattering angle, backgrounds from the furnace are completely eliminated by appropriate collimation.

TGA data were taken using a Perkin–Elmer TGA-7 system. On both heating and cooling, the temperature was ramped at 2°C/min to the first hold temperature and then held for about 2–10 hr until the weight of sample was no longer changing. The temperature was then ramped at 2°C/min to the next hold temperature, and the process was repeated until the final temperature was reached.

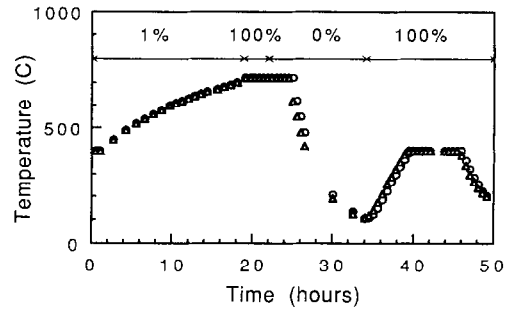

FIG. 1. A real-time representation of the sequence of neutron powder diffraction data sets taken on $Ba_{0.6}K_{0.4}BiO_y$ during the *in situ* experiment. Each data set was collected for about 28 min. The circles and triangles represent, respectively, the initial and final temperatures of the sample during the collection of each data set. The oxygen partial pressure of the flowing gas in the sample chamber is indicated above by the numbers.

III. *In situ* Neutron Powder Diffraction Results

A large number of diffraction data sets were collected during the *in situ* NPD experiment. The sequence of experimental conditions (temperature, oxygen partial pressure, and waiting time) for this experiment is shown schematically in Fig. 1. The sample was first heated from room temperature to 720°C in a flowing gas with $P_{O_2} = 1\% P_{total}$, where P_{total} is about 1 bar. The temperature was then held at 720°C while the flowing gas was changed from 1% O_2 to 100% O_2, and then to argon. Subsequently, the sample was cooled in argon to about 130°C, followed by an anneal in 100% O_2 at 400°C. Because of time limitations, the sample in the NPD experiment may not be fully in equilibrium with the furnace environment. However, the deviation from the equilibrium conditions is expected to be small. As will be seen later, the temperatures at which phase transformations were observed in the NPD experiment coincide well with the temperatures at which weight anomalies were observed in the TGA data (which more closely monitors the equilibrium phase behavior). Since much of the NPD data were taken while the sample temperature was changing, plots of raw data shown later will be labeled with the temperature range rather than a single temperature.

a. On Heating in 1% O_2

Figure 2 shows raw NPD data collected as the $Ba_{0.6}K_{0.4}BiO_3$ sample was heated from room temperature to 720°C in 1% O_2. The

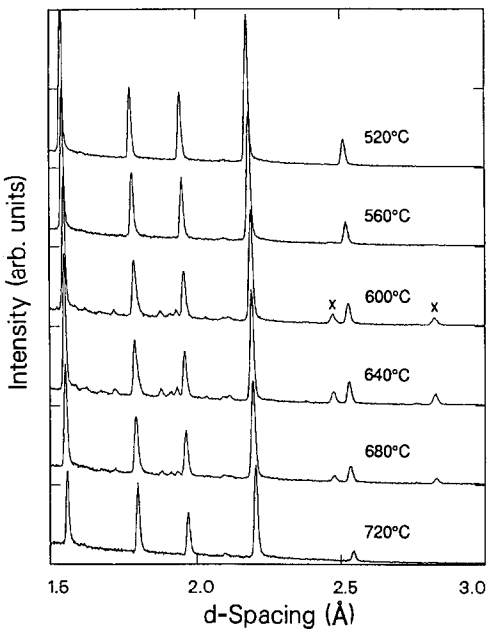

FIG. 2. Selected raw neutron powder diffraction data collected while heating $Ba_{0.6}K_{0.4}BiO_y$ in 1% O_2. Two major diffraction peaks of the $KBiO_2$ phase are indicated by x.

material retains a cubic perovskite structure at all temperatures. However, above 560°C, a second phase is observed to form and coexist with the perovskite phase. The fraction of this second phase increases with increasing temperature to 640°C, and then decreases with further temperature increase. At 720°C, the sample is again a single-phase cubic perovskite, but contains a large concentration of oxygen vacancies.

The second phase is $KBiO_2$ (*7*). The NPD data can be accurately modeled using two-phase Rietveld refinement (*8*) to give the composition and the relative abundance (from the ratio of the refined scale factors) for the two phases. The changes of these parameters as a function of temperature are shown in Fig. 3. As the sample is heated, oxygen vacancies form in the cubic perovskite phase. Vacancy formation continues monotonically until 560°C, at which point $KBiO_2$ begins to form as a second phase. As $KBiO_2$ is formed, the potassium content in the cubic perovskite phase decreases and its oxygen content increases. This chemical phase separation process continues until 640°C, at which point potassium begins to be reincorporated into the cubic perovskite

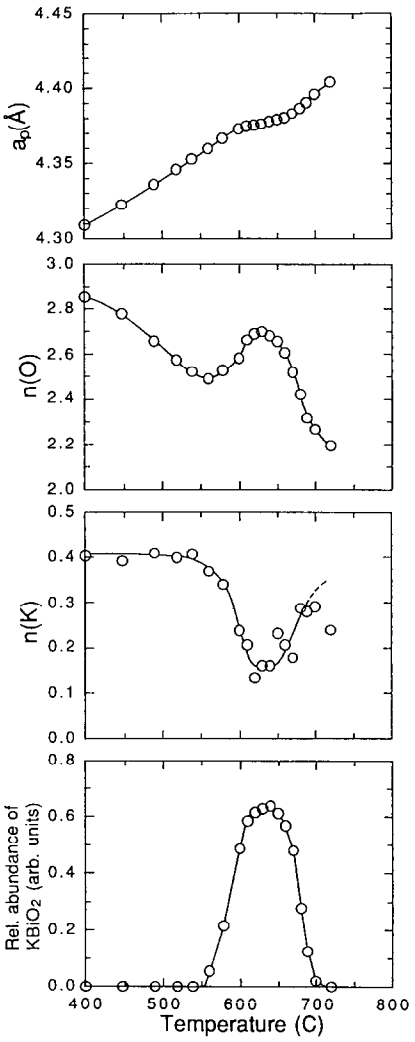

FIG. 3. Refined relative abundance of the $KBiO_2$ phase, the potassium and oxygen composition, and lattice parameter, a_p, of the cubic perovskite phase as a function of temperature on heating $Ba_{0.6}K_{0.4}BiO_y$ in 1% O_2.

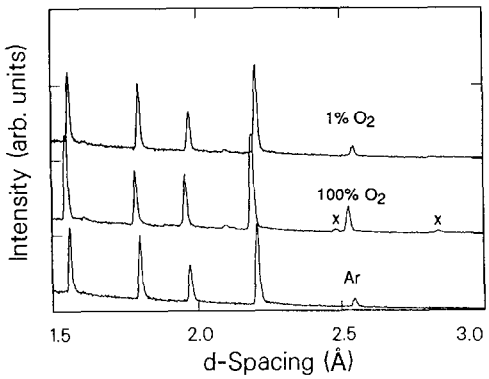

FIG. 4. Raw neutron powder diffraction data for $Ba_{0.6}K_{0.4}BiO_y$ at 720°C in three different oxygen partial pressures. Two major diffraction peaks of the $KBiO_2$ phase are indicated by *x*.

phase at the expense of $KBiO_2$. This process is accompanied by a rapid decrease in the oxygen content of the cubic perovskite phase. At 720°C, all of the potassium is reincorporated, resulting in a single-phase cubic perovskite material.

The lattice parameter, a_p, of the cubic perovskite phase as a function of temperature is also shown in Fig. 3. a_p initially increases almost linearly with temperature (at a rate of $\sim 7 \times 10^{-5}$ K^{-1}). The variation of a_p with temperature, however, is much larger than the normal thermal expansion (1×10^{-5} K^{-1}) at room temperature (*9*). We conclude that a large fraction of the lattice expansion observed on heating results from the loss of oxygen that reduces Bi^{+5} cations to form the larger Bi^{+3} cations. In the temperature range where two phases coexist, the change in a_p deviates from this linear behavior. Here, the competing effects of thermal expansion (increasing a_p), oxygen loss (increasing a_p), and potassium loss (decreasing a_p (*9*)) produce a shallow dip as shown in Fig. 3.

b. At 720°C in Different Oxygen Partial Pressures

Figure 4 shows raw NPD data from $Ba_{0.6}K_{0.4}BiO_y$ at 720°C in three different oxygen partial pressures. As shown above, $Ba_{0.6}K_{0.4}BiO_y$ is a single-phase cubic perovskite at 720°C in 1% O_2. When the flowing gas was changed to 100% O_2, $KBiO_2$ was observed to form as a second phase in the sample. The decomposition reaction is fully reversible at this temperature since all the potassium was reincorporated when the flowing gas was changed to pure argon. These data show that at the typical synthesis temperature (720°C) the solubility of potassium in the perovskite phase increases as the oxygen partial pressure decreases.

c. On Cooling in Argon and in Subsequent Reoxygenation

Figure 5 shows raw NPD data from the $Ba_{0.6}K_{0.4}BiO_y$ sample on cooling from 720°C in argon. A complex diffraction pattern developed below 620°C and persists to the lowest temperature (130°C) investigated, but no $KBiO_2$ was observed at any temperature. Thus, the chemical phase separation observed previously in 1% O_2 was prevented by cooling the sample in argon. Subsequent heating of this sample in pure oxygen near 250°C converted the phase with the complex diffraction pattern to the cubic perovskite phase, as shown in Fig. 6. The cell edge of the cubic perovskite phase at room tempera-

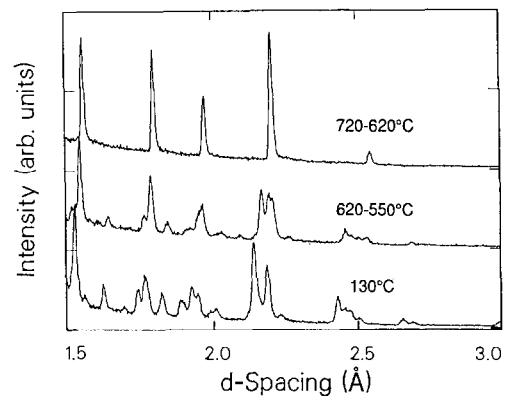

FIG. 5. Raw neutron powder diffraction data collected while cooling $Ba_{0.6}K_{0.4}BiO_{\sim 2.3}$ in pure argon.

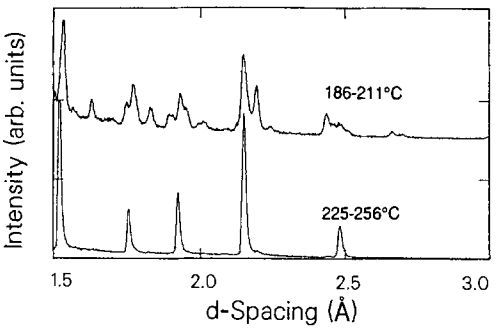

FIG. 6. Raw neutron powder diffraction data collected while heating $Ba_{0.6}K_{0.4}BiO_{\sim 2.3}$ in 100% O_2 to 400°C for reoxygenation.

ture was 4.2885(1) Å, very close to the initial value, 4.2892(1) Å, measured before the *in situ* experiment. Therefore, we conclude that we have fully recovered the $Ba_{0.6}K_{0.4}BiO_3$ material after the *in situ* NPD experiment.

The NPD pattern of the oxygen-deficient phase resulting from cooling in argon can be indexed using an orthorhombic cell of $a = \sqrt{2}a_p$, $b = 2\sqrt{2}a_p$, and $c = a_p$, where a_p is the edge of the simple cubic perovskite unit cell. Based on 31 resolved Bragg peaks, the observed extinction conditions are $0kl$, $k = 2n$; $h0l$, $h = 2n$; $h00$, $h = 2n$; $0k0$, $k = 2n$. Thus, the allowed space groups are the centrosymmetric space group *Pbam* and the noncentrosymmetric space group *Pba*2. Refinements were carried out using *Pbam*. This yielded a satisfactory fit to the NPD data, as shown in Fig. 7. Further refinements using the noncentrosymmetric space group *Pba*2 did not improve the fit significantly; thus, the *Pbam* structure was adopted. The refined structural parameters and atom–atom distances are given in Tables I and II, respectively. Similar structures have been observed in $LaCuO_{2.5}$ (*10*) and $CaMnO_{2.5}$ (*11*).

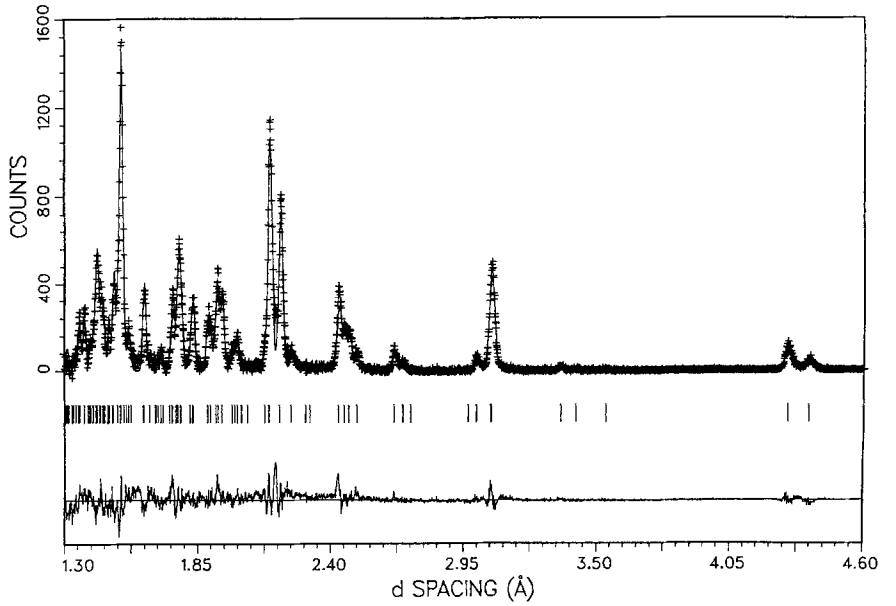

FIG. 7. Portion of the Rietveld refinement profile for the oxygen-vacancy-ordered $Ba_{0.6}K_{0.4}BiO_{\sim 2.3}$ phase at about 130°C. Plus marks (+) are the raw data. The solid line is the calculated profile. Tick marks below the profile mark the positions of the allowed reflections. A difference curve (observed minus calculated) is plotted at the bottom. Background has been fit as part of the refinement but subtracted prior to plotting.

TABLE I

STRUCTURAL PARAMETERS FOR THE OXYGEN-VACANCY-ORDERED $Ba_{0.6}K_{0.4}BiO_{\sim 2.3}$ PHASE AT 130°C

Atom	Site	x/a	y/b	z/c	B (Å^2)	Occupancy
Ba/K	4*g*	0.800(1)	0.1390(7)	0	2.7(2)	0.6/0.4
Bi	4*h*	0.2838(6)	0.1146(4)	0.5	1.5(1)	1
O_1	4*g*	0.301(1)	0.1149(8)	0	4.9(3)	0.71(2)
O_2	4*h*	0.081(1)	0.2459(5)	0.5	4.1(3)	0.98(2)
O_3	2*b*	0	0	0.5	3.3(4)	0.51(2)
O_4	2*d*	0	0.5	0.5	=B(O_3)	0.05(1)

Note. Space group orthorhombic *Pbam* (#55); a = 6.1163(5) Å, b = 11.995(1) Å, and c = 4.3705(2) Å; Z = 4; R_{wp}/R_{exp} = 0.121/0.071. A total of 537 reflections covering a d-space range from 0.71 to 5.5 Å is included in the refinement. Numbers without uncertainties are not refined.

The structure of the orthorhombic $Ba_{0.6}K_{0.4}BiO_y$ phase is illustrated in Fig. 8. It is a layered structure formed from one BiO_z ($z \approx 1.5$) layer and one $(Ba_{0.6}K_{0.4})O_z$ ($z \leq 1$) layer. In the BiO_z layer, oxygen atoms are arranged to produce a nearly completely ordered $\sqrt{2}a_p \times 2\sqrt{2}a_p$ configuration with alternating filled and half-filled oxygen chains. Bi atoms are relaxed toward neighboring oxygen vacancies. This leads to a short Bi–Bi distance (3.8 Å) across the vacancies compared with the case where two Bi atoms are bonded through an intermediate oxygen atom (~4.4 Å). Similar behavior has been observed by Beyerlein *et al.* (*12*) in the oxygen-deficient pyrochlores $Pb_2Ru_2O_{6.5}$ and $PbTlNb_2O_{6.5}$, where the Pb–Pb distance is reduced for Pb atoms on opposite sites of an oxygen vacancy. The refined overall oxygen content, y = 2.25(4), indicates that all Bi cations are in the 3+ state in this phase. It is interesting to note that the net charges on either the BiO_z (z = 1.53) layer or the $(Ba_{0.6}K_{0.4})O_z$ (z = 0.71) layer are quite small. This suggests that at low temperature the oxygen vacancies tend to be distributed in a way that achieves charge neutrality for each individual layer.

TABLE II

INTERATOMIC DISTANCES (Å) IN THE OXYGEN-VACANCY-ORDERED $Ba_{0.6}K_{0.4}BiO_{\sim 2.3}$ PHASE AT 130°C

$(Bi–Bi)_{O_1}$	4.3704(2)	Bi–O_1	2.1878(6)
$(Bi–Bi)_{O_2}$	4.461(6)	Bi–O_2	2.005(8)
$(Bi–Bi)_{O_3}$	4.429(8)		2.470(8)
$(Bi–Bi)_{O_4}$	3.815(8)	Bi–O_3	2.215(4)
Ba(K)–O_1	2.95(1)	Bi–O_4	1.908(4)
Ba(K)–O_2	2.613(7)		

Note. Distinct oxygen atoms bridging two Bi atoms are indicated by subscripts.

In a separate experiment where a $Ba_{0.6}K_{0.4}BiO_y$ ($y \approx 2.3$) sample was quenched from 720°C in nitrogen, we found that the sample at room temperature contains a mixture of the cubic phase and the $\sqrt{2}a_p \times 2\sqrt{2}a_p \times a_p$ orthorhombic phase. Therefore, as expected, the $\sqrt{2}a_p \times 2\sqrt{2}a_p \times a_p$ oxygen vacancy ordering can be suppressed by quenching. However, the potassium distribution in the sample is still homogeneous. Following an oxygen anneal at 400°C, the sample becomes a single-phase cubic perovskite with sharp diffraction peaks.

V. Thermogravimetric Analysis

The phase separation involving $KBiO_2$ observed in NPD data can also be detected by thermogravimetric measurements. Figure 9 shows the TGA data taken as a

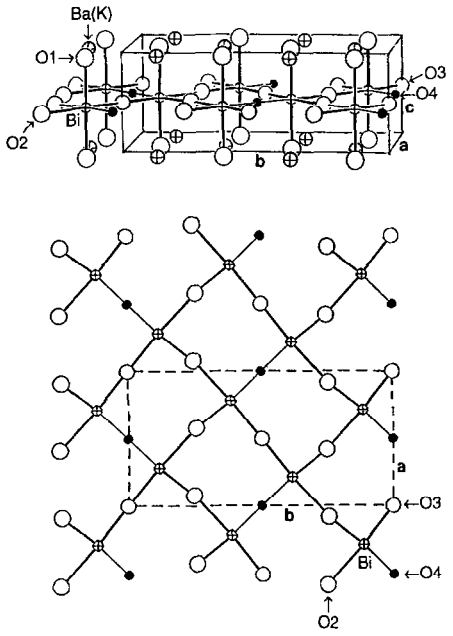

FIG. 8. Structure of the oxygen-vacancy-ordered $Ba_{0.6}K_{0.4}BiO_{\sim 2.3}$ phase: top—the full unit cell; bottom—the details of the oxygen vacancy ordering in the $BiO_{\sim 1.5}$ layer (as viewed along the c-axis). The solid circles indicate the vacant O_4 sites.

$Ba_{0.6}K_{0.4}BiO_y$ sample is heated in 1% O_2. The starting material is fully oxygenated ($y = 3.0$). On heating, the weight of this sample initially decreases due to the formation of oxygen vacancies in the single-phase perovskite. It then exhibits a plateau over the temperature range 560–650°C, where $KBiO_2$ forms as a second phase. Physically, this means that the total oxygen content in the sample is nominally constant in this temperature range. This is in agreement with the NPD observation that the oxygen vacancy concentration in the perovskite phase decreases while $KBiO_2$ is forming as a second phase. Above this temperature range, the weight of the sample decreases rapidly as the potassium is reincorporated by the perovskite phase. At 720°C, the sample is a single-phase perovskite.

In the temperature range (<560°C and >720°C) where the material is single-phase, the oxygen content of the perovskite phase can be determined from the weight loss of the sample. The calculated oxygen contents can be found from Fig. 9, referring to the right y-axis. As the temperature is increased above 720°C, we expect that the oxygen content should approach asymptotically to $y = 2.3$, where all Bi atoms have a formal oxygenation state of 3+. In addition, we note that the values of oxygen content in the two single-phase temperature ranges can be smoothly jointed together as shown by the dashed line in Fig. 9. On the other hand, in the temperature range where two phases coexist (560–720°C), the calculated oxygen contents must be interpreted as an average over the entire sample.

It should be pointed out that the compositions of the perovskite phase obtained by refining NPD data are subject to some systematic errors at elevated temperature. At room temperature, the composition ($x = 0.40$ and $y = 2.98$) from Rietveld refinement of NPD data agrees well with the known chemical composition of the $Ba_{0.6}K_{0.4}BiO_3$ sample. However, at elevated temperature, the refined values for oxygen contents are consistently smaller than the values obtained by TGA. For example, at 720°C, where the single-phase perovskite is pres-

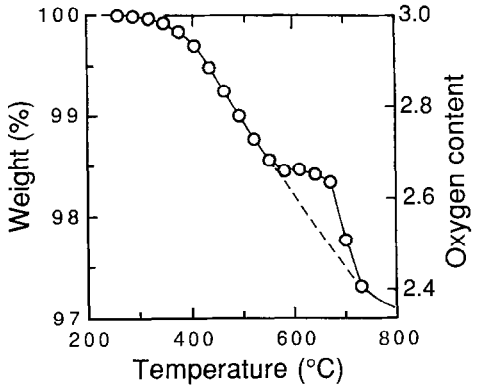

FIG. 9. TGA weight loss and the calculated average oxygen content of the $Ba_{0.6}K_{0.4}BiO_y$ sample on heating in 1% O_2.

ent, the refined oxygen content ($y = 2.19$) is smaller than the value ($y = 2.4$) calculated from the TGA weight loss. Also, the refined potassium content of the perovskite phase is smaller than $x = 0.40$ at 720°C, where the sample is single-phase. One possible source for such systematic errors is the correlation between refined atom site occupancies and temperature factors that become very large and may be anharmonic at high temperature. Another possible source of error is the thermal diffuse scattering background in the NPD data, which may not be adequately modeled at high temperature in the present refinements. We observed appreciable diffuse scattering in the low d-space range at high temperature.

VI. Phase Diagram

The NPD data collected from $Ba_{0.6}K_{0.4}BiO_y$ on heating show a novel reentrant phase behavior as the temperature increases. The material at this potassium content is a single-phase perovskite at low temperature (<560°C), a mixture of the perovskite and $KBiO_2$ phases in the intermediate temperature (560–720°C), and the single-phase perovskite again at high temperature (>720°C). It is important to determine whether this reentrant behavior is an equilibrium phenomenon or simply a kinetic effect due to slow potassium diffusion at low temperature. Hinks *et al.* found that the weight of a $Ba_{0.6}K_{0.4}BiO_3$ samples does not return to its initial value after being heated and then cooled at 1°C/min in 100% O_2 (*13*) and 1% O_2 (*14*). After such thermal cycling, a large residual weight loss ($\Delta y \approx 0.3$) occurs. This indicated that the final material contains $KBiO_2$, which has a lower oxygen content than the perovskite phase, as a second phase. Accordingly, the phase change at 560°C seen in the present NPD data on heating may correspond to an irreversible decomposition of a metastable phase.

The work by Hinks *et al.* concerning the stability of $Ba_{0.6}K_{0.4}BiO_3$ is not conclusive. Assuming that the potassium diffusion kinetics is slow below 560°C, the $x = 0.4$ material may not have sufficient time to incorporate the potassium into a single-phase perovskite lattice at the cooling rate used in their work (*13, 14*). We have therefore performed additional experiments to clarify the previous work.

In a TGA experiment, a $Ba_{0.6}K_{0.4}BiO_3$ sample was first heated from room temperature to 720°C in 1% O_2, equilibrated at 720°C for about 2 hr, and then cooled to 400°C. Here, an unusually long cooling time (6 days) was used to minimize the possible deviation of this sample from its equilibrium phase behavior. Again, a large weight loss ($\Delta y = 0.32$) was found in the final sample at 400°C, compared with the weight of the starting material. This showed that the phase separation observed around 560°C in 1% O_2 on heating is not a reversible phase change.

In another experiment, a single-phase $Ba_{0.6}K_{0.4}BiO_3$ sample was heated to 510°C in 1% O_2, and then held at 510°C for 11 days. Although this temperature was 50°C below the phase separation temperature determined on heating from the previous NPD experiment, the sample was found to have decomposed into a mixture of the perovskite phase and $KBiO_2$, as shown in Fig. 10. This perovskite phase exhibits $\sqrt{2}a_p \times \sqrt{2}a_p \times 2a_p$ superlattice reflections, consistent with those supercell phases observed in the low potassium concentration range in $Ba_{1-x}K_xBiO_3$ (*9*). The composition of this perovskite phase was estimated to be $Ba_{0.81}K_{0.19}BiO_3$ based on its lattice parameters. Thus, we conclude that the $Ba_{0.6}K_{0.4}BiO_3$ perovskite is a metastable phase at low temperature. On heating, the single-phase perovskite tends to decompose into a similar perovskite with a smaller potassium content and $KBiO_2$. At low temperatures, however, the phase separation of this material is hindered by sluggish potassium diffusion kinetics.

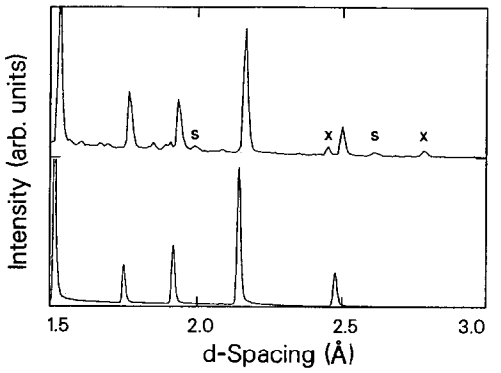

FIG. 10. Raw neutron powder diffraction data at room temperature for a $Ba_{0.6}K_{0.4}BiO_3$ sample: bottom—the initial sample was a single-phase perovskite; top—the sample decomposes into a mixture of $Ba_{0.81}K_{0.19}BiO_3$ and $KBiO_2$ after being annealed at 510°C in 1% O_2 for 11 days. The major diffraction peaks for the $KBiO_2$ phase are indicated by x and the $\sqrt{2}a_p \times \sqrt{2}a_p \times 2a_p$ superlattice perovskite peaks by s (*9*).

Figure 11 shows a schematic phase diagram of $Ba_{1-x}K_xBiO_y$ in 1% O_2. The full curve represents the equilibrium potassium solubility line. Above 640°C, this curve is essentially the same as the plot of n(K) vs T as shown in Fig. 3. We note from Fig. 3 that the potassium solubility is reduced to 0.15 near 640°C. The dashed curve in Fig. 11 represents changes in the potassium content of perovskite phase as the $Ba_{0.6}K_{0.4}BiO_3$ sample decomposes on heating (*14*). The above results show that this dashed curve is not an equilibrium phase line, but a metastability line for the $x = 0.4$ composition. The primary feature of this phase diagram is the presence of the single-phase oxygen-deficient perovskite region at high temperature and a mixed-phase region (perovskite + $KBiO_2$), at lower temperature above $x = 0.1$. The solubility of potassium in the perovskite phase decreases with decreasing temperature in the high-temperature range. Also, as the oxygen partial pressure increases at fixed temperature, the solubility of potassium in the perovskite phase decreases. According to NPD data at 720°C, the $Ba_{0.6}K_{0.4}BiO_y$ sample is single-phase in 1% O_2 and argon, but it is a mixture of the perovskite and $KBiO_2$ in 100% O_2.

Because of the occurrence of phase separation involving $KBiO_2$ at low temperature, it is clear that the superconducting compositions ($x > 0.37$) (*9*) cannot be retained in the perovskite phase if the sample is slowly cooled in an atmosphere containing O_2. This result could explain early failures in preparing the superconducting material of $Ba_{1-x}K_xBiO_3$ in either O_2 or air (*1–3*). In order to make the superconducting material, it is necessary to suppress this phase separation during cooling. It is noted that the occurrence of this phase separation on cooling requires a large oxygen intake (refer to TGA data in the temperature range 560–720°C in Fig. 9). Therefore, this phase separation can be suppressed by quenching the material to low temperature, avoiding an appreciable oxygen intake. Particularly, slow cooling (~1°C/min) in the NPD experiment suppresses this chemical phase separation since

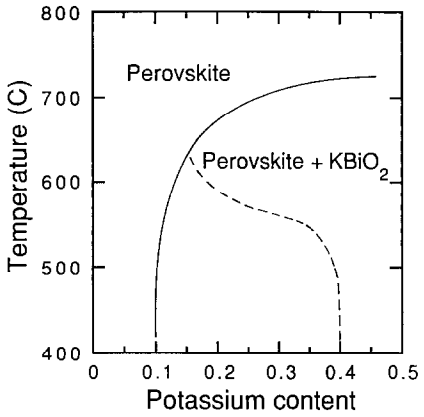

FIG. 11. Schematic high-temperature phase diagram for the $Ba_{1-x}K_xBiO_y$ system in 1% oxygen partial pressure. The full curve represents the equilibrium phase boundary. The dashed curve (i.e., the metastability line) indicates the potassium content in the perovskite phase as a $Ba_{0.6}K_{0.4}BiO_3$ material is heated and forms $KBiO_2$ (*14*).

in this case the inert atmosphere contains no oxygen.

VII. Conclusions

This work gives important insight into the synthetic chemistry of superconducting $Ba_{1-x}K_xBiO_3$. Most importantly, we know that the material at superconducting compositions is metastable. The method used to synthesize this material may be applicable to other new oxide superconductors.

The solubility of potassium in the perovskite $Ba_{1-x}K_xBiO_y$ is controlled by temperature and oxygen partial pressure. Beyond the solubility limit, $KBiO_2$ is formed as a second phase. The potassium solubility increases at high temperature and decreases with increasing oxygen partial pressure. In general, the potassium solubility decreases with increasing oxygen vacancy concentration. The arrangement of the oxygen vacancies in the crystal lattice, either random or ordered, is not important for the incorporation of the potassium into the perovskite phase. Thus, the concentration of oxygen vacancies can be regarded as a key parameter that determines the potassium solubility. Such a hypothesis can be understood in terms of the chemical oxidation state of Bi in the compound. The formation of oxygen vacancies compensates for the substitution of Ba^{2+} by K^{1+} and sets the overall oxidation state of Bi $(x + 2y - 2)$ below some maximum value. In contrast, the substitution of Bi by Pb in $BaPb_xBi_{1-x}O_3$ is not expected to require the formation of oxygen vacancies, since in this case the oxidation state of Bi is not raised by the Pb substitution. This could explain why single-phase material can be synthesized in oxygen for $BaPb_xBi_{1-x}O_3$ over the entire doping range $(0 \leq x \leq 1)$ but not for $Ba_{1-x}K_xBiO_3$ (*15*).

Acknowledgments

This work is supported by the National Science Foundation, Science and Technology Center for Superconductivity, under Grant DMR-88-09854 (S.P., D.R.R., B.D.), the U.S. Department of Energy, Basic Energy Sciences–Materials Sciences, under Contract number W-31-109-ENG-38 (J.D.J., D.G.H., Y.Z., A.W.M.).

References

1. L. F. Mattheiss, E. M. Gyorgy, and D. W. Johnson, Jr., *Phys. Rev. B* **37,** 3745 (1988).
2. R. J. Cava, B. Batlogg, J. J. Krajewski, R. C. Farrow, L. W. Rupp, Jr., A. E. White, K. T. Short, W. F. Peck, Jr., and T. Y. Kometani, *Nature* **332,** 814 (1988).
3. D. G. Hinks, B. Dabrowski, J. D. Jorgensen, A. W. Mitchell, D. R. Richards, Shiyou Pei, and Donglu Shi, *Nature* **333,** 836 (1988).
4. D. G. Hinks, A. W. Mitchell, Y. Zheng, D. R. Richards, and B. Dabrowski, *Appl. Phys. Lett.* **54,** 1595 (1989).
5. J. D. Jorgensen, *in* "Chemical Crystallography with Pulsed Neutrons and Synchrotron X-Rays" (M. A. Carrondo and G. A. Jeffrey, Eds.), pp. 159–184, Vol. 221, NATO ASI Series C: Mathematical and Physical Sciences, Reidel, Dordrecht (1988).
6. J. D. Jorgensen, J. Faber, Jr., J. M. Carpenter, R. K. Crawford, J. R. Haumann, R. L. Hitterman, R. Kleb, G. E. Ostrowski, F. J. Rotella, and T. G. Worlton, *J. Appl. Crystallogr.* **22,** 321 (1989).
7. B. Schwedes and R. Z. Hoppe, *Z. Anorg. Allg. Chem.* **392,** 97 (1972).
8. R. B. VonDreele, J. D. Jorgensen, and C. G. Windsor, *J. Appl. Crystallogr* **15,** 581 (1982).
9. Shiyou Pei, J. D. Jorgensen, B. Dabrowski, D. G. Hinks, D. R. Richards, and A. W. Mitchell, *Phys. Rev. B* **41,** 4126 (1990).
10. J. F. Bringley, B. A. Scott, S. J. Laplaca, R. F. Boehme, T. M. Shaw, M. W. McElfresh, S. S. Trail, and D. E. Cox, *Nature* **347,** 263 (1990).
11. K. R. Poeppelmeier, M. E. Leonowicz, J. C. Scanlon, J. M. Longo, and W. B. Yelon, *J. Solid State Chem.* **45,** 71 (1982).
12. R. A. Beyerlein, H. S. Horowitz, J. M. Longo, M. E. Leonowicz, J. D. Jorgensen, and F. J. Rotella, *J. Solid State Chem.* **51,** 253 (1984).
13. D. G. Hinks, D. R. Richards, B. Dabrowski, A. W. Mitchell, J. D. Jorgensen, and D. T. Marx, *Physica C* **156,** 477 (1988).
14. D. G. Hinks, J. D. Jorgensen, D. R. Richards, Ying Zheng, A. W. Mitchell, Shiyou Pei, and B. Dabrowski, *J. Less-Common Met.* **168,** 19 (1991).
15. A. W. Sleight, J. L. Gillson, and P. E. Bierstedt, *Solid State Commun.* **17,** 27 (1975).